

Approximate Theory of Four-Point Alternating Current Potential Drop on a Flat Metal Surface

Nicola BOWLER, Yongqiang HUANG

*Iowa State University, Center for Nondestructive Evaluation,
Applied Sciences Complex II, 1915 Scholl Road, Ames Iowa 50011, USA.*

Abstract. An analytical expression for the voltage measured by a four-point alternating current potential drop (ACPD) method on a flat metal surface is derived. Far-field expressions for the electric field in a metal plate and in the region of the probe (air) are used to obtain contributions to the ACPD voltage from the metal plate and due to inductance in the pick-up circuit. The far-field approximation is accurate for a plate whose edges are several tens of skin depths from the probe, and for a probe whose pick-up points are several skin depths away from the current drive points. Comparison of the theory with experiment on a brass plate shows excellent agreement.

1 Introduction

The alternating current potential drop (ACPD) method measures the voltage, \mathcal{V} , between two pick-up points on the surface of a conductor. For the configuration shown in Figure 1,

$$\mathcal{V} = V + \varepsilon = - \int_{(p,y,0)}^{(q,y,0)} \mathbf{E} \cdot d\mathbf{l} + \oint_C \mathbf{E} \cdot d\mathbf{l}, \quad (1)$$

where C is a closed loop, l is the vertical height of the pick-up loop above the plate surface and ε is the rate of change of magnetic flux within the loop [1].

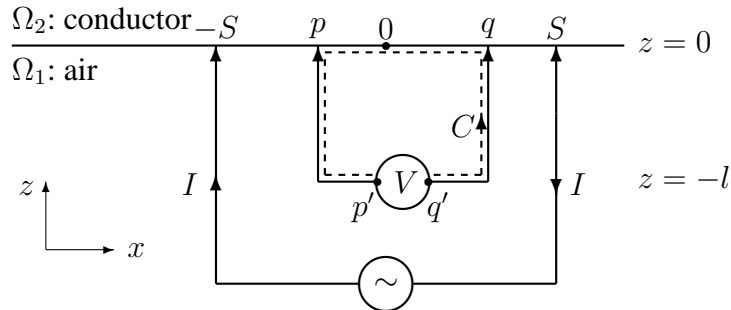


Figure 1: Path of integration, C (- - -), may occupy any plane of constant y . Here the plane $y = 0$ is shown.

In direct current potential drop measurements there is no induction effect in the measurement circuit ($\varepsilon = 0$) since the current does not vary with time. The measured potential drop is almost exclusively due to the conductor. In ACPD measurements, the contribution to \mathcal{V} from

the conductor dominates when the frequency is sufficiently low, since the inductive contribution from the measurement circuit, $i\omega L$, is proportional to frequency ω . At sufficiently high frequency the inductive term dominates. This technique is similar to resistivity measurement methods used in applied geophysics, although the latter are usually performed at low frequency and interpreted in the limit of direct current [2].

In this work, both contributions to \mathcal{V} are evaluated. The far-field approximation for \mathbf{E} is used in calculating \mathcal{V} . This approximation gives accurate results when pick-up points at $(p, y, 0)$ and $(q, y, 0)$ are sufficiently far from the source points at $(\pm S, 0, 0)$, in practice a few electromagnetic skin depths (δ) in the conductor.

2 Electric Field

For the configuration shown in Figure 1, the electric field can be obtained by superposition of fields separately associated with the two current-carrying wires:

$$\mathbf{E}^T(\mathbf{r}) = \mathbf{E}(\mathbf{r}_+) - \mathbf{E}(\mathbf{r}_-), \quad (2)$$

where $r_{\pm} = \sqrt{(x \pm S)^2 + y^2 + z^2}$. In the following sections the far-field form of \mathbf{E} is determined in the region of the pick-up circuit (air) and in the metal plate for a *single* current-carrying wire located on the axis of a cylindrical co-ordinate system.

2.1 Probe Region

For a single wire passing current I into, or out of, a conductive plate, there are two contributions to the electric field in air. One is from the current flowing in the wire, \mathbf{E}^w , and the other is from the current density in the plate. In the far-field regime, for the closed loop C , only \mathbf{E}^w is important. Assuming that the wire is perpendicular to the surface of the plate and that the current has time-dependence $e^{-i\omega t}$, the integral form of Ampère's Law and then Faraday's Law yields

$$\mathbf{E}^w(\rho, z) = \hat{z} \frac{i\omega\mu_0 I}{2\pi} \ln \rho, \quad \rho \rightarrow \infty, z \leq 0, \quad (3)$$

where ρ is the radial co-ordinate of a cylindrical system centered on the wire and \mathbf{E}^w has the same direction as the current density in the wire, $\mathbf{J} = \hat{z}J_z$.

2.2 Plate

An expression for the electric field in the conductive plate is obtained in a manner similar to that given in reference [3] for a conductive half-space. For a current source oriented perpendicular to the surface of the plate, only the transverse magnetic (TM) potential, ψ'' , is required to fully describe the electric field:

$$\mathbf{E}(\mathbf{r}) = -i\omega\mu\nabla \times \nabla \times \hat{z}\psi''(\mathbf{r}). \quad (4)$$

Define a modified TM potential

$$\Psi = \nabla_z^2 \psi'', \quad (5)$$

where $\nabla_z \equiv \nabla - \hat{z}(\partial/\partial z)$ is the transverse differential operator. For a plate infinite in x and y , occupying $z \in [0, T]$, the governing equation is

$$(\nabla^2 + k^2)\Psi(\mathbf{r}) = 0, \quad 0 \leq z \leq T, \quad (6)$$

where $k^2 = i\omega\mu\sigma$ with μ and σ being the permeability and conductivity of the plate, respectively. In the plate, only the horizontal component of the electric field, E_ρ , contributes to V . It is not convenient to express E_ρ in terms of Ψ . Rather, E_ρ will be obtained from the following equation by means of relationship (5).

$$E_\rho(\mathbf{r}) = -i\omega\mu \frac{\partial^2 \psi''(\mathbf{r})}{\partial \rho \partial z}, \quad (7)$$

where ρ and z are co-ordinates of the cylindrical system. Equation (6) is solved for Ψ subject to boundary conditions

$$\Psi(\rho, 0) = C(\rho) \quad \text{where} \quad C(\rho) = \begin{cases} \frac{I}{\pi(ka)^2}, & \rho \leq a, \\ 0, & \rho > a, \end{cases} \quad (8)$$

and

$$\Psi(\rho, T) = 0. \quad (9)$$

These derive from the fact that, at the surface of the plate, the normal component of current density is continuous - zero everywhere apart from at the point of contact with the current-carrying wire, radius a . Applying the zero-order Hankel transform to solve (6) and taking the limit $a \rightarrow 0$ yields

$$\Psi(\rho, z) = \frac{I}{2\pi k^2} \int_0^\infty e^{-\gamma z} \left[\frac{1 - e^{2\gamma(z-T)}}{1 - e^{-2\gamma T}} \right] J_0(\kappa\rho) \kappa d\kappa, \quad (10)$$

where $\gamma^2 = \kappa^2 - k^2$. If $T \rightarrow \infty$, the term in square brackets tends to unity and the resulting integral is identical to that obtained for a half-space conductor [3].

It is possible to evaluate the integral in (10) analytically by expanding the term in the denominator as a binomial series [5, 3.6.10]:

$$(1 - e^{-2\gamma T})^{-1} = 1 + e^{-2\gamma T} + e^{-4\gamma T} + e^{-6\gamma T} + e^{-8\gamma T} + \dots = \sum_{n=0}^{\infty} e^{-2n\gamma T}. \quad (11)$$

Multiplying the right-hand side of (11) by the factor $e^{-\gamma z}[1 - e^{2\gamma(z-T)}]$, and substituting the result into (10), yields

$$\Psi(\rho, z) = \frac{I}{2\pi k^2} \sum_{n=0}^{\infty} \int_0^\infty \{ e^{-\gamma(z+2nT)} - e^{\gamma[z-2(n+1)T]} \} J_0(\kappa\rho) \kappa d\kappa, \quad (12)$$

where the order of summation and integration has been reversed. The first term in braces in (12), $e^{-\gamma z}$, gives rise to the result for the TM potential in a half-space conductor. The second term, $-e^{\gamma(z-2T)}$, accounts for the primary reflection of the field from the surface of the plate at $z = T$. Other terms deal with multiple reflections between the surfaces of the plate. By analogy with the result for the half-space conductor, reference [3], or by multiple use of the analytic result given in reference [6], result 8.2.23, the terms in (12) can be integrated. It is found that

$$\Psi(\rho, z) = -\frac{I}{2\pi} \sum_{n=0}^{\infty} \left\{ \frac{ik(z+2nT)}{(ikr_n)^3} e^{ikr_n} (1 - ikr_n) + \frac{ik[z-2(n+1)T]}{(ikr'_n)^3} e^{ikr'_n} (1 - ikr'_n) \right\}, \quad 0 \leq z \leq T, \quad (13)$$

wherein $r_n = \sqrt{\rho^2 + (z + 2nT)^2}$ and $r'_n = \sqrt{\rho^2 + [z - 2(n + 1)T]^2}$. To obtain E_ρ from Ψ as given in (13) via relations (7) and (5) requires some manipulation [3]. The result is

$$E_\rho(\mathbf{r}) = -\frac{ikI}{2\pi\sigma\rho} \sum_{n=0}^{\infty} \left\{ e^{ik(z+2nT)} - \frac{e^{ikr_n}}{ikr_n} \left[1 + \frac{[ik(z + 2nT)]^2}{ikr_n} \left(1 - \frac{1}{ikr_n} \right) \right] \right. \\ \left. + e^{-ik[z-2(n+1)T]} - \frac{e^{ikr'_n}}{ikr'_n} \left[1 + \frac{\{ik[z - 2(n + 1)T]\}^2}{ikr'_n} \left(1 - \frac{1}{ikr'_n} \right) \right] \right\}, \quad 0 \leq z \leq T. \quad (14)$$

In the far field, the electric field is dominated by terms of the form e^{ikz}/ρ and

$$E_\rho(\mathbf{r}) = -\frac{ikI}{2\pi\sigma\rho} \sum_{n=0}^{\infty} \{e^{ik(z+2nT)} + e^{-ik[z-2(n+1)T]}\}, \quad \rho \rightarrow \infty, 0 \leq z \leq T. \quad (15)$$

If the far-field current density is integrated over a cylindrical surface of large radius extending from $z = 0$ to T , the result is $I[1 + e^{ik(2N+1)T}]$ for a series truncated to N terms. This expression tends to I as $N \rightarrow \infty$, as it should. If $T \rightarrow \infty$ the far-field expression for the electric field in a half-space conductor is recovered [3]

$$E_\rho(\mathbf{r}) = -\hat{\rho} \frac{ikI}{2\pi\sigma\rho} e^{ikz}, \quad \rho \rightarrow \infty, z \geq 0. \quad (16)$$

This expression was also given in reference [4] in the context of fatigue crack measurement.

3 Voltage calculation

Voltage is now calculated according to equation (1). For the configuration shown in Figure 1 the contributions are

$$\mathcal{V} = V + \varepsilon = -\int_p^q E_x^T(x, y, 0)dx + \int_0^{-l} E_z^T(p, y, z)dz + \int_{-l}^0 E_z^T(q, y, z)dz, \quad (17)$$

with \mathbf{E}^T given by (2). It is a simple matter to evaluate the last two terms on the right-hand side of equation (17) with E_z given in equation (3). To neatly evaluate the first term on the right-hand side of (17) recognize that, at the surface defined by $z = 0$, equation (15) can be written

$$E_\rho(\rho, 0) = -\frac{ikI}{2\pi\sigma\rho} \left[\left(2 \sum_{n=0}^{\infty} e^{2iknT} \right) - 1 \right], \quad \rho \rightarrow \infty. \quad (18)$$

Further [5, equation 3.6.10],

$$\sum_{n=0}^{\infty} e^{2iknT} = \frac{1}{1 - e^{2ikT}},$$

so that

$$E_\rho(\rho, 0) = \frac{ikI}{2\pi\sigma\rho} \coth(ikT), \quad \rho \rightarrow \infty. \quad (19)$$

The final expression for \mathcal{V} is

$$\mathcal{V} = \frac{I}{4\pi} \left[-\frac{ik}{\sigma} \coth(ikT) + i\omega\mu_0 l \right] \ln \left\{ \left[\frac{(p - S)^2 + y^2}{(p + S)^2 + y^2} \right] \left[\frac{(q + S)^2 + y^2}{(q - S)^2 + y^2} \right] \right\}. \quad (20)$$

Table 1: Experimental parameters.

brass plate		probe (Figure 1)	
conductivity, σ (MSm^{-1})	16.2 ± 0.3	S (mm)	38.2 ± 0.3
thickness, T (mm)	5.66 ± 0.01	p (mm)	-9.18 ± 0.01
horizontal dimensions (mm)	615×616	q (mm)	9.18 ± 0.01
		l (mm)	0.35 (fitted value)

The first term in equation (20) is the contribution from the conductor and has approximately equal real and imaginary parts. The contribution from the measurement circuit is imaginary (inductive) and proportional to the dimension of the circuit perpendicular to the conductor surface, l . For a typical non-magnetic metal and $l \sim 1$ mm, the inductive term is practically negligible for frequencies up to about 10 Hz whereas at 10^4 Hz the terms are of similar magnitude. The logarithmic term represents the physical arrangement of the four probe points.

4 Experiment

ACPD measurements were made as a function of frequency on a brass plate whose conductivity and dimensions are given in Table 1. The brass plate was precision ground to remove surface scratches and mounted on a 5 cm thick plastic support plate. Electrical contact with the brass plate was made via sprung, point contacts, held perpendicular to the surface of the plate. In this experiment the four contact points were arranged in a straight line, with a common midpoint between the two current drive points and the two pick-up points. The dimensions of the probe are given in Table 1.

The two current-carrying wires were held perpendicular to the plate surface for a distance of approximately 40 cm, after which they were twisted together to reduce the effects of inter-wire capacitance. This distance was sufficient to remove any effect of motion of the current wires on the measured voltage. The two pick-up wires were arranged with the objective of minimizing l , lying as close to the plate surface as possible. They were twisted together at the midpoint between the pick-up points.

In the theoretical calculation, two measured values are needed. One is the current through the plate, the other is the voltage measured by the pick-up probe. To monitor the current in the plate, a high precision resistor was connected in series with the drive current circuit and the voltage across the resistor measured. The resistance maintains one percent accuracy over the range of frequency for which it could be measured with an Agilent 4294A precision impedance analyzer; 40 Hz to 40 kHz. The voltage across the resistor and that of the pick-up probe were both measured using a Stanford Research Systems SR830 DSP lock-in amplifier. In order to make both voltage measurements using the same lock-in amplifier, a switch was used activated by a control signal from the auxiliary analog output of the lock-in amplifier.

It was necessary to correct the experimental data for common-mode rejection (CMR) error in the lock-in amplifier. This systematic error shows itself by the fact that, when the pick-up terminals are reversed, the measured voltage changes by a few μV . The magnitude of the error is, therefore, similar to that of the voltage being measured, and a corrective procedure is essential. The CMR error was eliminated by taking two sets of measurements, reversing the pick-up terminals for the second. The two sets were then subtracted and the result divided by two.

The drive current was produced by a Kepco bipolar operational power supply/amplifier,

model number BOP 20-20M. The sine signal from the internal function generator of the lock-in amplifier was connected to the current programming input of the power supply, with the power supply working as a current drive.

The conductivity of the plate was measured using a MIZ-21A eddy current instrument. The error quoted in Table 1 is estimated from the manufacturer's literature and derives from a combination of inaccuracy in the instrument, inaccuracy in the comparative standards and probe lift-off error.

In Figure 2, ACPD measurements are compared with theory. The average of ten data sets (taken sequentially) is shown. The value of l was adjusted in the calculation to obtain the best fit to the high frequency part of the data, having negligible influence on the low-frequency data. The value $l = 0.35$ mm appears reasonable since the pick-up wire is AWG 32 with diameter 0.2 mm. The agreement between theory and experiment is excellent. There is no obvious error in the imaginary part of \mathcal{V} . The theory overestimates the low frequency real part of \mathcal{V} by 3%. Applying standard error analysis to the low frequency limiting expression for \mathcal{V} , equation (22), shows that errors in the plate conductivity and in the relative positions of the probe points combine to give an experimental error which is also 3%.

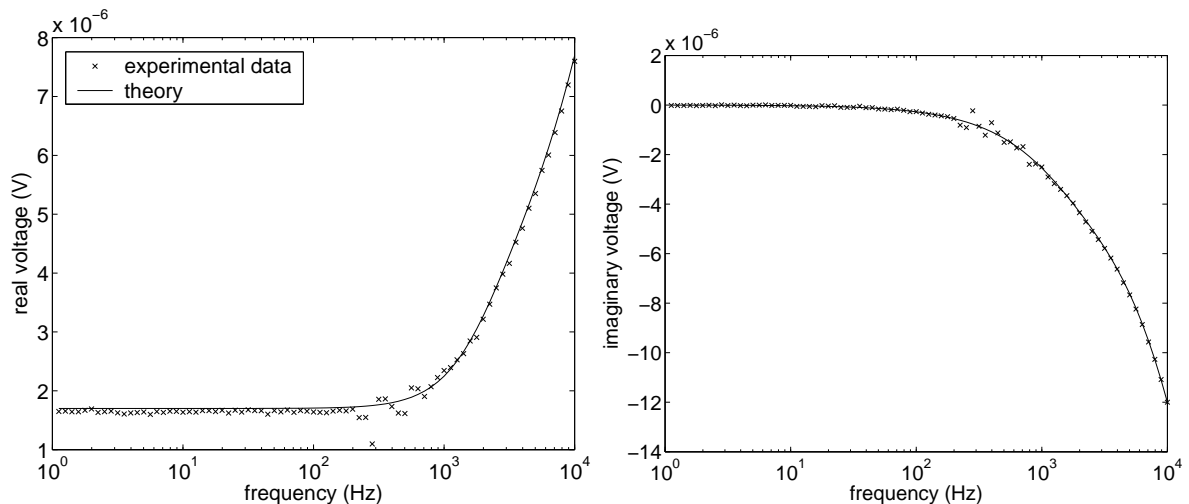


Figure 2: ACPD measurements on a brass plate compared with theory, equation (20). Experimental parameters are given in Table 1.

5 Limiting Cases

5.1 Half Space Conductor

If the limit $T \rightarrow \infty$ is taken in equation (20), $\coth(ikT) \rightarrow -1$ and \mathcal{V} for a half-space conductor is given by

$$\mathcal{V} = \frac{I}{4\pi} \left(\frac{ik}{\sigma} + i\omega\mu_0 l \right) \ln \left\{ \left[\frac{(p-S)^2 + y^2}{(p+S)^2 + y^2} \right] \left[\frac{(q+S)^2 + y^2}{(q-S)^2 + y^2} \right] \right\}. \quad (21)$$

Considering the behavior of $\coth(x)$, it can be shown that the plate thickness needs to be only twice the electromagnetic skin depth in order for the plate to behave as a half-space, to within 1% accuracy. In Figure 3, \mathcal{V} is plotted for a number of values of plate thickness, including a half-space. The calculations are made using equations (20) and (21). For the plate

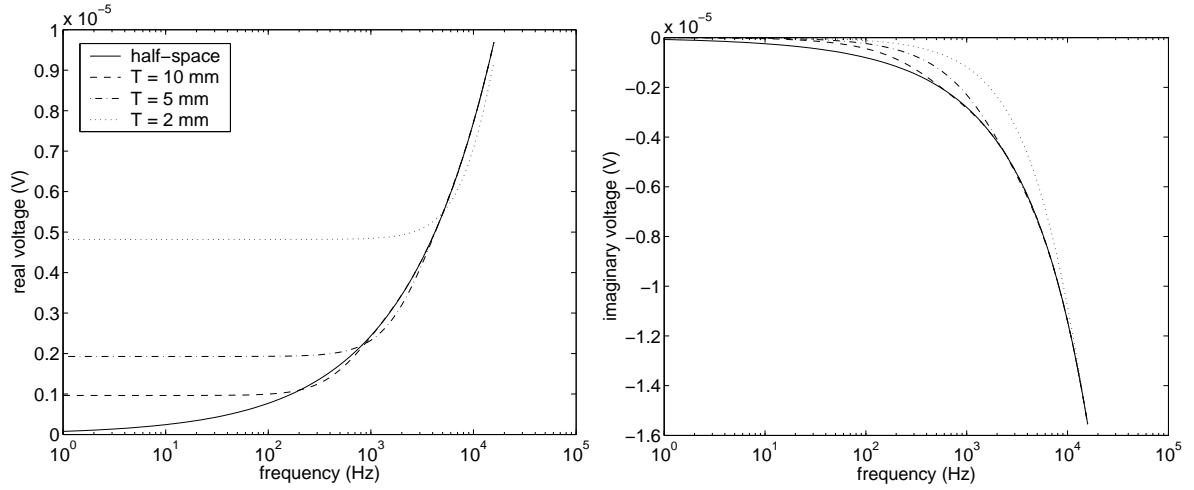


Figure 3: Calculated values of \mathcal{V} as a function of frequency and plate thickness. Other parameters are given in Table 1.

with thickness 10 mm, the frequency at which $T = 2\delta$ is about 600 Hz. It can be seen from Figure 3 that the theory for the half-space and the plate converge at this point, as expected.

5.2 Low Frequency

To take the limit $k \rightarrow 0$ in equation (20), note that $\lim_{k \rightarrow 0} [ikT / \sinh(ikT)] = 1$. Then

$$\mathcal{V} \rightarrow -\frac{I}{4\pi\sigma T} \ln \left\{ \left[\frac{(p-S)^2 + y^2}{(p+S)^2 + y^2} \right] \left[\frac{(q+S)^2 + y^2}{(q-S)^2 + y^2} \right] \right\}, \quad k \rightarrow 0. \quad (22)$$

It is seen that at low frequency the voltage is real, being inversely proportional to the plate thickness and conductivity. Formula (22) is consistent with one given by Yamashita and Masahiro for four-point DC measurements on a finite plate [7]. The inverse dependence of $\text{Re}(\mathcal{V})$ on the plate thickness at low frequency, predicted by equation (22), can be clearly seen in Figure 3.

5.3 High Frequency

At high frequency the voltage is dominated by the inductive term in equation (20). This term is proportional to l , the length of the pick-up wire perpendicular to the metal plate. Practically it is desirable to minimize the contribution of this term by making l as small as possible. In this way the contribution to \mathcal{V} due to the plate, from which useful information may be derived, is not masked by induction in the measurement circuit. In Figure 4, the effect on \mathcal{V} of varying l is shown. Only $\text{Im}(\mathcal{V})$ is shown since l has no influence on $\text{Re}(\mathcal{V})$.

6 Conclusion

This simple analytic result, equation (20), gives useful insight into the primary contributors in ACPD measurements. It is accurate for a flat metal plate whose edges are several tens of skin depths from the probe, and for a probe whose pick-up points are several skin depths away

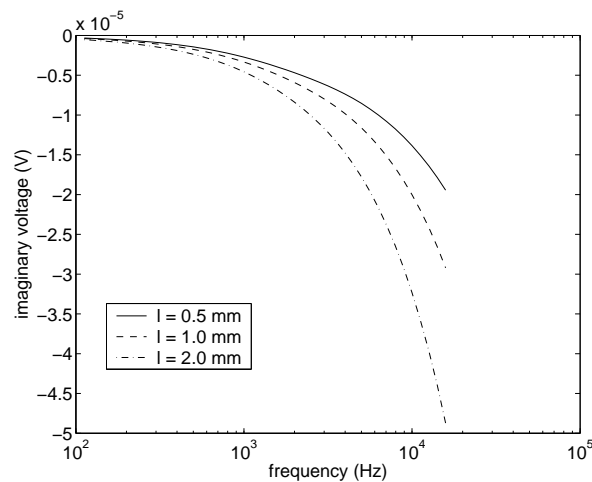


Figure 4: Calculated values of $\text{Im}(\mathcal{V})$ as a function of frequency and perpendicular length of the pick-up wire, l . Other parameters are given in Table 1.

from the current drive points. Near-field contributions to \mathcal{V} and surface layers are subjects of future work.

Acknowledgment

This work was supported by the NSF Industry/University Cooperative Research program. The authors would like to thank Marcus Johnson and John Bowler for helpful comments regarding the experiment.

References

- [1] W. J. Duffin, *Electricity and Magnetism*, McGraw-Hill, London, 1980. 3rd Edition.
- [2] D. S. Parasnis, *Principles of Applied Geophysics*, Chapman and Hall, London, 1997. 5th Edition.
- [3] N. Bowler, Analytical Solution for the Electric Field in a Half Space Conductor Due to Alternating Current Injected at the Surface, *J. Appl. Phys.* **95** (2004) 344-348.
- [4] V. G. Gerasimov, A. D. Kovachev, Yu. V. Kulaev and A. D. Pokrovskii, An Analysis of the Operation of a Transducer with Contact Excitation in Fatigue Tests of Flat Samples, *Defektoskopiya*, **1** (1981) 21-32.
- [5] M. Abramowitz and I. A. Stegun (eds.), *Handbook of mathematical functions with formulas, graphs and mathematical tables*. Dover, New York, 1972.
- [6] A. Erdélyi (ed.), *Tables of integral transforms Vol. II*. McGraw-Hill, New York, 1954.
- [7] M. Yamashita and M. Agu, Geometrical correction factor for semiconductor resistivity measurements by four-point probe method, *Japanese J. Appl. Phys.* **23** (1984) 1499-1504.